

FeS₂ monolayer: A high-valence and high- T_C Ising ferromagnetKe Yang,^{1,2,*} Yaozhenghang Ma^{2,*}, Lu Liu,² Yueyue Ning,¹ Di Lu,² Yuxuan Zhou,² Zhongyao Li,¹ and Hua Wu^{2,3,4,†}¹College of Science, University of Shanghai for Science and Technology, Shanghai 200093, China²Laboratory for Computational Physical Sciences (MOE), State Key Laboratory of Surface Physics, and Department of Physics, Fudan University, Shanghai 200433, China³Shanghai Qi Zhi Institute, Shanghai 200232, China⁴Collaborative Innovation Center of Advanced Microstructures, Nanjing 210093, China

(Received 24 September 2023; revised 21 December 2023; accepted 11 January 2024; published 26 January 2024)

Two-dimensional (2D) magnetic materials are currently of great interest for their promising applications in spintronics. Strong magnetic coupling and anisotropy are both highly desirable for the achievement of high-temperature magnetic order. Here we propose the unusual high-valence FeS₂ hexagonal monolayer as such a candidate for a strong Ising 2D ferromagnet by spin-orbital state analyses, first-principles calculations, and the renormalized spin-wave theory (RSWT). We find that, very importantly, the high-valence Fe⁴⁺ ion is in the low-spin state (t_{2g}^4 , $S = 1$) with degenerate t_{2g} orbitals rather than the high-spin state ($t_{2g}^3e_g^1$, $S = 2$). It is the low-spin state that allows us to carry a large perpendicular orbital moment and then produces a huge single-ion anisotropy (SIA) of 25 meV/Fe. Moreover, the negative charge-transfer character associated with the unusual high valence, strong Fe 3d-S 3p hybridization, wide bands, and a small band gap all help to establish a strong superexchange. Indeed, our first-principles calculations confirm the strong ferromagnetic superexchange and the huge perpendicular SIA, both of which are further enhanced by a compressive strain. Then, our RSWT calculations predict that the ferromagnet T_C is 261 K for the pristine FeS₂ monolayer and could be increased to 409 K under -5% compressive strain. The high T_C is also reproduced by our Monte Carlo simulations. Therefore, it is worth exploring high- T_C Ising ferromagnets in high-valence 2D magnetic materials with degenerate orbitals.

DOI: [10.1103/PhysRevB.109.014431](https://doi.org/10.1103/PhysRevB.109.014431)**I. INTRODUCTION**

Since the discovery of the two-dimensional (2D) ferromagnets CrI₃ [1] and Cr₂Ge₂Te₆ [2] in 2017, 2D magnetic materials have attracted great interest due to their promising applications in quantum devices and information technology [3–7]. According to the Mermin-Wagner theorem [8], magnetic anisotropy (MA) is essential for establishing long-range magnetic order in 2D materials. Both the CrI₃ monolayer [1] and Cr₂Ge₂Te₆ bilayer [2] have a weak perpendicular MA, which was ascribed to an exchange anisotropy caused by the spin-orbit coupling (SOC) of the heavy ligand p orbitals and their hybridization with the Cr 3d orbitals [9–11]. Here the octahedral Cr³⁺ $S = 3/2$ ion has a closed t_{2g}^3 shell, and its orbital singlet produces no single-ion anisotropy (SIA). In contrast, the VI₃ monolayer has an open V³⁺ t_{2g}^2 shell, which allows for an unquenched orbital moment and a large SIA of 16 meV per V³⁺ ion [12]. This accounts for the recent experimental observations of the large orbital moment and Ising magnetism in the VI₃ monolayer [13–15]. As a large MA maintains a preferred magnetic orientation against the thermal fluctuation and excitation, it may stabilize long-range magnetic order at a high temperature [1, 2, 13–20]. To facilitate practical applications of 2D magnetic materials, it is highly desirable to achieve both

strong magnetic coupling and anisotropy in them and thus their high ordering temperature.

Very recently, an unusual high-valence FeS₂ monolayer in a triangular structure was successfully synthesized using a competitive-chemical-reaction-based growth mechanism [21]. Its main structural units are the edge-sharing FeS₆ octahedra arranged into a delicate triangular network of Fe ions, as seen in Fig. 1(a). It was found to be an intriguing 2D ferromagnetic (FM) semiconductor with a small band gap and a low Curie temperature ($T_C \approx 15$ K), and its analog with higher T_C may have potential applications in photodetectors and spintronic devices [21].

In contrast to a series of existing 2D magnetic materials with normal valence states such as Cr³⁺ in CrI₃ [1] and Mn²⁺ in MnBi₂Te₄ [22, 23], the FeS₂ monolayer is quite unique because of the unusual high-valence Fe⁴⁺ ions. High-valence transition metal (TM) compounds often have exotic electronic states, strong covalency between the TM and ligands, and surprising magnetic properties [24–26]. Although the Hund exchange favors a high-spin (HS) state with a maximal spin for 3d TM ions, such as Cr³⁺ $S = 3/2$, Mn²⁺ $S = 5/2$, Fe²⁺ $S = 2$, and Fe³⁺ $S = 5/2$, the octahedral Fe⁴⁺ ion may well be in a low-spin (LS) $S = 1$ state rather than the HS $S = 2$ state, as the very strong hybridization between Fe⁴⁺ 3d and S²⁻ 3p orbitals could dominate over the Hund exchange and as a result could stabilize the LS state. In addition, the strong hybridization and wide band effect would narrow the band gap of semiconductors or even produce a metallic

*These authors contributed equally to this work.

†Corresponding author: wuh@fudan.edu.cn

behavior, and all of this would favor magnetic couplings, either superexchange via the virtual excitation across the small band gap or the itinerant magnetism in metallic systems. Moreover, the formal LS Fe^{4+} ($3d^4$, $S = 1$) ion in the local FeS_6 octahedron has the $t_{2g}^{3\uparrow,1\downarrow}$ configuration, and the degenerate t_{2g} triplet orbitals could carry the large orbital moment $L = 1$ and produce a strong SIA. Then, the pristine FeS_2 monolayer could have both strong magnetic coupling and anisotropy, and consequently, it could possess a high ordering temperature suitable for promising spintronic applications. Furthermore, we rationalize the recent experimental low T_C by demonstrating the S vacancy effect below and thus propose that the native high T_C of FeS_2 monolayer may be restored by removing the S vacancies.

The above pictures motivate us to study the electronic structure and magnetic properties of the FeS_2 monolayer using first-principles calculations, the crystal field level and spin-state diagrams, charge-transfer-type superexchange analysis, and renormalized spin-wave theory (RSWT) calculations. Indeed, our work confirms that the unusual high-valence Fe^{4+} ion is in the LS $S = 1$ state and possesses a large out-of-plane orbital moment of about $1\mu_B$ and thus a huge perpendicular SIA of 25 meV/Fe. Moreover, we find that the FeS_2 monolayer is a charge-transfer-type semiconductor with a tiny band gap and has very strong FM couplings. Thus, the pristine FeS_2 monolayer would have quite high T_C which is even increased above room temperature under a few percent compressive strain according to our RSWT calculations and MC simulations. Therefore, this prediction calls for an experimental study, and high-valence van der Waals magnetic materials with degenerate orbitals are worth exploring in the search for 2D high- T_C Ising ferromagnets.

II. COMPUTATIONAL DETAILS

We perform density functional theory (DFT) calculations using the Vienna Ab initio Simulation Package (VASP) [27]. The kinetic energy cutoff for plane wave expansion is set to 500 eV. A Monkhorst-Pack grid of $11 \times 11 \times 1$ is used for the 1×1 planar unit cell, and a $(3 \times 3 \times 1)$ k mesh is used for the 4×4 planar supercell. The experimental lattice constants $a = b = 3.23 \text{ \AA}$ [21] for the FeS_2 monolayer are used in our calculations, as the DFT optimized lattice constants $a = b = 3.20 \text{ \AA}$ are almost the same as them. The atomic positions are fully relaxed until the force on each atom is less than 0.01 eV/\AA , and the total energy minimization is performed with a tolerance of 10^{-5} eV . A vacuum space larger than 15 \AA is employed to avoid periodic image interactions between FeS_2 layers. To account for the electron correlation of Fe $3d$ states, local-spin-density approximation plus Hubbard's U (LSDA + U) calculations are performed using the common value of Hubbard's $U = 5 \text{ eV}$ and Hund's exchange $J_H = 1 \text{ eV}$, and moreover, the hybrid functional calculations are carried out. Both the calculations give very similar band structures, as seen below, and also reproduce the experimental small gap. Furthermore, we test the U values in the reasonable range of 4–6 eV and find that our prediction of the quite high T_C Ising ferromagnet remains unchanged, as seen below.

To check the ground state and possible metastable states of the spin-orbital system, we use the open-source software

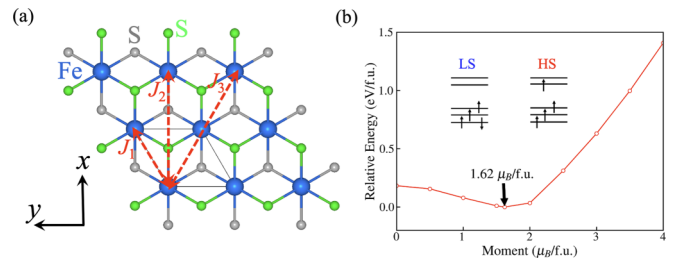


FIG. 1. (a) The crystal structure of the FeS_2 monolayer. J_1 , J_2 , and J_3 refer to the first-, second-, and third-nearest-neighbor magnetic exchanges. (b) Fixed-spin-moment calculations imply the formal low-spin state with $S = 1$ for Fe^{4+} .

developed by Watson [28] to construct the occupation number matrices for multiple spin-orbital states; more details are given in Sec. I of the Supplemental Material (SM) [29] (see also references [21,30–37] therein). Then, the LSDA + U calculations read those occupation number matrices and yield the orbitally dependent/polarized potential in each iteration of the electronic steps. Furthermore, those occupation number matrices are updated and read iteratively in self-consistent calculations until full electronic relaxation. Normally, in such calculations the ground state and several low-energy metastable states can be stabilized as they are, but some high-energy metastable states are too unstable to converge to the ground state or a low-energy metastable state. Then, one can determine the ground state of the spin-orbital system in a reliable way using such calculations, as demonstrated in many previous works [12,17,20,38,39]. For example, such calculations can well reproduce the experimental crystal field level splitting and orbital excitation energy, and in this work their accuracy is proven by reproducing the SOC strength of the Fe^{4+} $3d$ electrons, as seen below. Note also that the SOC is included for Fe and S atoms using the second-variational method with scalar relativistic wave functions. The magnetic phase transition of the FeS_2 monolayer is probed using RSWT and MC simulations; more computational details are given in the SM [29].

III. RESULTS AND DISCUSSION

A. The low-spin state of the Fe^{4+} ion

To clearly see the crystal field effect, exchange splitting, electron correlation, and crucial SOC effects, we present and discuss the LSDA and LSDA + SOC + U calculations. We first carry out LSDA calculations to see the basic electronic structure of the FeS_2 monolayer. The Fe $3d$ states in the local FeS_6 octahedron split into the higher-lying e_g^σ doublet and the lower t_{2g} triplet with an energy separation of about 2 eV, and t_{2g} further splits into the a_{1g} singlet and e_g^π doublet in the global trigonal crystal field, as seen in Fig. 2 and in Sec. I of the SM [29]. a_{1g} and e_g^π are almost degenerate and spin polarized, with the up-spin channel being fully filled but the down-spin one being partially occupied, and the e_g^σ doublet is formally unoccupied, with the antibonding state lying around 2 eV above the Fermi level. Obviously, there is strong hybridization between the Fe $3d$ and S $3p$ states, causing their broad bands to distribute over a large energy

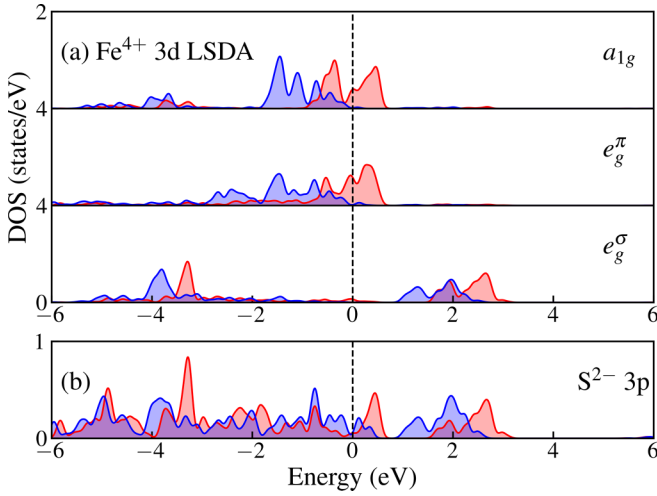


FIG. 2. (a) Fe $3d$ and (b) S $3p$ densities of states (DOSs) from the LSDA. The blue (red) curves stand for the up (down) spin channel. The Fermi level is set at zero energy.

range from -6 to 3 eV. It is the strong hybridization that produces a huge $pd\sigma$ bonding-antibonding splitting of about 6 eV (about -4 vs 2 eV) for the Fe $3d$ e_g^σ states. There are a lot of holes on the S $3p$ states, featuring the negative charge-transfer behavior in such unusually high valence compounds [40,41]. The calculated local spin moment is $1.50\mu_B$ per Fe⁴⁺, implying a low-spin $S = 1$ state with the formal $t_{2g}^{3\uparrow,1\downarrow}$ configuration. Owing to the strong Fe $3d$ -S $3p$ hybridization, the S $3p$ fat orbitals/delocalized states also get somewhat spin polarized, having $0.03\mu_B$ per S within their muffin-tin sphere and $0.06\mu_B$ in the interstitial region per formula unit (f.u.). All those spin moments add up to the total spin moment of $1.62\mu_B/\text{f.u.}$, but this moment is still reduced from the formal Fe⁴⁺ $S = 1$ state just by the electron itineracy in the LSDA metallic band structure originating from the strong Fe $3d$ -S $3p$ hybridization.

To double-check the possible LS ground state of the formal Fe⁴⁺ ion, we perform fixed-spin-moment calculations and compute the LSDA total energies for total spin moments ranging from the nonmagnetic $S = 0$ state via the LS $S = 1$ to the HS $S = 2$ state. As seen in Fig. 1(b), the obtained results show that the ground state indeed has a total spin moment close to $2\mu_B/\text{f.u.}$ (i.e., the LS $S = 1$ state) and that the HS $S = 2$ state is extremely unstable, lying too far above the LS state by about 1.5 eV/f.u. All of the above results show that the unusual high-valence Fe⁴⁺ ion is in the formal LS $S = 1$ state rather than the HS $S = 2$ state.

B. The $L_z = 1$ ground state and huge SIA

The LS Fe⁴⁺ ion has the formal $t_{2g}^{3\uparrow,1\downarrow}$ configuration, and the nearly degenerate a_{1g} and e_g^π orbitals in the global trigonal crystal field could make the Fe⁴⁺ ion stay in different orbital states, as seen in Fig. 3. Actually, all these states have the same full filling of the up-spin t_{2g} orbitals and differ only in the occupation of the down-spin t_{2g} , which is therefore used to label those states. The different combinations of the a_{1g} singlet and e_g^π doublet in the case of the corresponding

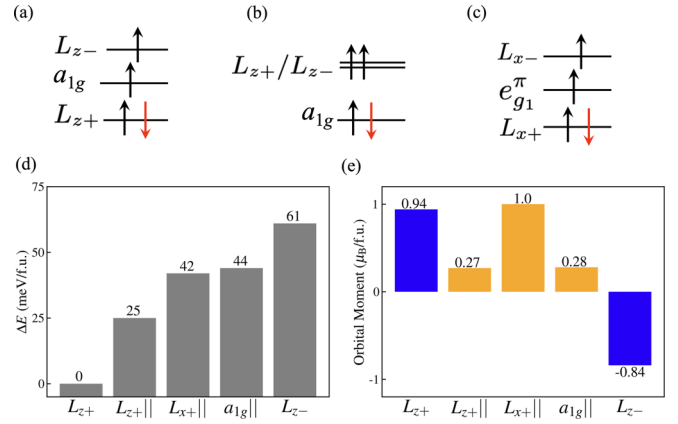


FIG. 3. Crystal field level diagrams for the LS Fe⁴⁺ $S = 1$ ion in different configuration states: the single down-spin electron occupies the (a) L_{z+} , (b) a_{1g} , and (c) L_{x+} states. (d) The relative total energies ΔE (meV/f.u.) and (e) orbital moments (blue for out of plane and yellow for in plane) for the FeS₂ monolayer in different states from LSDA + SOC + U . The symbol \parallel in the state labels marks the in-plane magnetization, in comparison with other states with out-of-plane magnetization.

orbital degeneracy yield the $L_{z\pm}$, $L_{x\pm}$, or $L_{y\pm}$ state with an orbital moment of $\pm 1\mu_B$ along the z , x , or y axis, respectively; see Sec. I of the SM for more details [29]. Note that the a_{1g} orbital singlet state in Fig. 3(b) formally has no orbital moment but could carry a small one due to the SOC mixing of a_{1g} and e_g^π . Moreover, owing to the actual trigonal crystal field splitting between the a_{1g} singlet and e_g^π doublet, the real $L_{z\pm}$ and $L_{x\pm}$ states obtained below could have an orbital moment different from $\pm 1\mu_B$ which is also spin orientation dependent due to the SOC effect [see Fig. 3(e)]. By including the SOC and electron correlation effects of Fe $3d$ orbitals, we carry out LSDA + SOC + U calculations to determine which state in Fig. 3(d) is the spin-orbital ground state of the FeS₂ monolayer. Indeed, all these states can be stabilized in our calculations guided by the initialized occupation number matrices and by the subsequent full electronic relaxation.

All the solutions are semiconducting with a tiny band gap, and the corresponding results are displayed in Fig. 4 and Sec. II in the SM [29]. The ground state is L_{z+} . It has a total spin moment of $1.98\mu_B$ and a parallel orbital moment of $0.94\mu_B$, both along the z axis [Figs. 3(a) and 4]. The L_{z-} state, where the orbital moment is antiparallel to the total spin moment, would lose the SOC energy, and the increasing total energy of 61 meV/f.u. [$\Delta E = \zeta(\Delta L_z)s_z = \zeta \times 2 \times 1/2$] leads to an estimate of the SOC parameter of $\zeta = 61$ meV for the formal Fe⁴⁺ ion [see Fig. 3(d)]. As the L_{z+} orbital moment firmly fixes, via the SOC, the parallel spin moment along the z axis, if the spin moment can be flipped into the xy plane, the total energy will rise by 25 meV/f.u. [Fig. 3(d)], showing a huge SIA energy of 25 meV/Fe which approaches the ideal $\zeta/2$. Moreover, we obtain the L_{x+} state, and it has both an x -axis spin moment of $2\mu_B$ and an orbital moment of $1\mu_B$, but its total energy is higher than the L_{z+} ground state by 42 meV/f.u. [see Figs. 3(d) and 3(e)]. We also get the a_{1g} state, and it has a finite in-plane orbital moment of $0.28\mu_B$ and lies above the L_{z+} ground state by 44 meV/f.u.

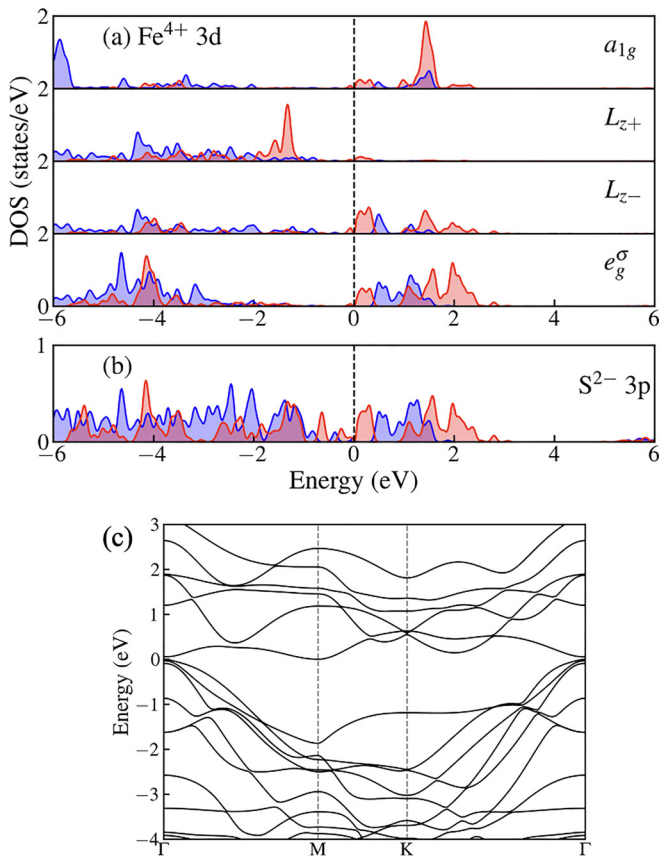


FIG. 4. (a) Fe 3d and (b) S 3p DOS of FeS₂ monolayer in the L_{z+} ground state by LSDA + SOC + U . The blue (red) curves stand for the up (down) spin channel. The Fermi level is set at zero energy. (c) The corresponding band structure with a tiny band gap of 40 meV.

Then, in the FeS₂ monolayer, the formal Fe⁴⁺ ion is in the low-spin t_{2g}^4 state with $S = 1$ and $L_z = 1$, and those occupied states are separated from other unoccupied Fe 3d states by electronic Coulomb correlations, which essentially determine the insulating behavior of the FeS₂ monolayer [see Fig. 4(a)]. The negative charge-transfer character and strong Fe 3d-S 3p hybridization, both associated with the unusually high Fe⁴⁺ valence state, give rise to broad bands which eventually reduce the above gap drastically to a minor semiconducting gap, as seen in Figs. 4(b) and 4(c).

Indeed, the energy splitting between the L_{z+} and L_{z-} orbitals arises from the SOC effect. In addition to this, electron correlation plays a significant role in determining the energy splitting between the occupied and unoccupied Fe 3d states, as shown in Fig. 4(a). In this work, we stabilize the spin-orbital ground state and several metastable states using LSDA + SOC + U calculations, where the “large” energy splitting between the occupied and unoccupied Fe 3d states is always present due to Hubbard’s U . In order to determine the spin-orbital excitation energy of the Fe 3d states, e.g., the L_{z+}/L_{z-} orbital splitting by SOC, we cannot use the DOS results and instead use the computed total energy differences, as shown in Fig. 3(d). Our results show that the SOC L_{z+}/L_{z-} splitting is 61 meV, which just reflects the SOC strength ζ of the Fe 3d state. Actually, the ζ parameter of the ionic Fe

3d state is known to be about 60–70 meV, and the present agreement reflects the good accuracy of our calculations.

After investigating all the spin-orbital states of the unusual high-valence and LS Fe⁴⁺ ions, we find that the ground state is L_{z+} [see Fig. 3(a)]. It has a nominal large orbital moment of $1\mu_B$ which is parallel to the total spin moment of $2\mu_B$ and has a small insulating gap of 40 meV, as shown in Fig. 4(c), which is in agreement with the observed small gap insulating behavior of the FeS₂ monolayer [21]. Note that this small gap band structure [Fig. 4(c)] is also well reproduced by a hybrid functional calculation which yields a very similar band structure, as seen in Fig. S6 in the SM [29]. Moreover, the L_{z+} ground state has a huge SIA energy of 25 meV/Fe and strongly favors perpendicular magnetization. Therefore, the FeS₂ monolayer could be an emerging 2D Ising magnet.

C. FM couplings and high T_C

We now study the magnetic properties of the FeS₂ monolayer. Besides the above calculated FM state, we also calculate three different antiferromagnetic (AFM) states, which are depicted in Fig. S7 in the SM [29]. All the calculations are based on the LS L_{z+} spin-orbital ground state. The results show that the FM solution is the ground state, and the three exchange parameters $J_1 = 5.81$ meV, $J_2 = 2.01$ meV, and $J_3 = 1.05$ meV are all FM; see Sec. IV in the SM for more details [29]. For 2D FM semiconductors and insulators, normally, a superexchange plays a dominant role in establishing the magnetic couplings, and the hybridization between the magnetic transition metal ions and the ligand ions has a strong impact on the strength of the superexchange couplings. The largest, $J_1 = 5.81$ meV, can be qualitatively explained by the charge-transfer-type superexchange, and the large distance J_3 of 1.05 meV is still sizable due to the strong Fe 3d-S 3p hybridization and the tiny band gap (in this unusually high valence system), both of which facilitate the long-range FM coupling. As the FeS₂ monolayer is a tiny-gap charge-transfer semiconductor, the virtual excitations from S 3p to Fe 3d associated with the superexchange are energetically cheap. Moreover, the strong Fe 3d-S 3p hybridizations yield large hopping parameters. Then the two major superexchange channels, including the large $pd\sigma$ and medium $pd\pi$ hybridizations, contribute to the FM J_1 coupling; for more details see Sec. V in the SM [29].

Using the three FM exchange parameters and the huge SIA parameter $D = 25$ meV, here we perform RSWT calculations (see Sec. VI in the SM [29]) and find that the FeS₂ monolayer has a pretty high $T_C = 261$ K, as seen in Fig. 5. In the RSWT calculations, T_C is sensitive to the SIA energy, and T_C will drop a lot when the SIA parameter is reduced from the present huge value of 25 meV down to the more common value of a few meV or a few tenths of a meV: e.g., T_C is reduced to 132 K for SIA = 2.5 meV and to 37 K for SIA = 0.25 meV (see Fig. 5). These results show that the present huge SIA indeed contributes a lot to stabilize the pretty high $T_C = 261$ K. Note that when using the three FM parameters ($J_1 = 4.73$ meV, $J_2 = 1.33$ meV, and $J_3 = 1.27$ meV; see Table S7 in the SM) and the unchanged $D = 25$ meV, both obtained using LSDA + SOC + U with $U = 6$ eV, T_C is somewhat reduced to 234 K. When $U = 4$ eV is assumed, the small gap is closed, and the

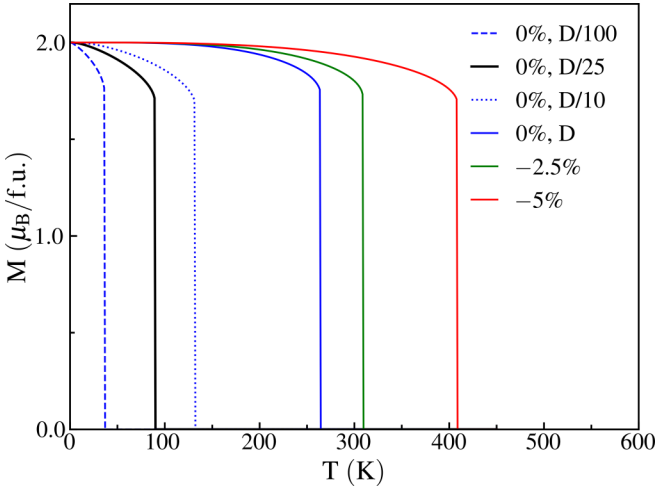


FIG. 5. The magnetization M as a function of temperature calculated with the RSWT. Here the SIA parameter is $D = 25$ meV. T_C is determined by $M = 0$.

FM metallic solution has a stronger itinerant FM behavior and higher $T_C > 261$ K (compared with $U = 5$ eV). Therefore, for the very reasonable $U = 5$ eV (or somewhat larger U) to open the experimental small gap of the FeS₂ monolayer, T_C must be 261 K (or somewhat lower but still a pretty high T_C).

As the SIA arises from the LS L_{z+} ground state which benefits from the half-filled lower e_g^π doublet rather than the a_{1g} singlet in the global trigonal crystal field, one would expect that a biaxial compressive strain would force the FeS₆ octahedra to elongate along the global z axis, i.e., along the local cubic [111] direction, and then enlarge the crystal field splitting between the lower e_g^π doublet and the higher a_{1g} singlet. As a result, the LS L_{z+} ground state, out of the lower e_g^π doublet, would become even more stable, and the in-plane FM exchange could become stronger due to the shortened bond lengths. Upon biaxial compressive strain, the energy separation between the L_{z+} ground state and the higher a_{1g} singlet is, indeed, increased as expected (see Fig. S9 in the SM [29]), but under tensile strain, the energy separation is reduced and even changes sign when the tensile strain is larger than 2.5%. Moreover, under compressive strain, the FM ground state becomes more stable than other AFM states, indicating a stronger FM exchange; see Sec. VII in the SM for more details [29]. Then, using the enhanced FM exchanges and the huge SIA under compressive strain, our RSWT calculations show that T_C is increased from 261 K for the pristine FeS₂ monolayer to 310 K for -2.5% strain and to 409 K for -5.0% strain (see Fig. 5). We also carry out MC simulations and find T_C is comparable to the RSWT prediction. The corresponding T_C values are 220, 275, and 350 K according to our MC simulations; see Sec. VIII in the SM [29]. Both sets of results arrive at the same conclusion that the pristine FeS₂ monolayer will have a pretty high T_C which is even above room temperature under a few percent compressive strain. Therefore, the emerging FeS₂ monolayer could be an appealing high- T_C 2D Ising ferromagnet.

D. Sulfur vacancy

Now we comment on why the recent experimental T_C is only about 15 K [21]. It may well be due to the S vacancies.

Such ligand vacancies are quite common in high-valence materials [26,42,43] and 2D materials [44–47]. We performed DFT calculations using a 3×3 supercell with a single sulfur vacancy in our simulations (with a vacancy ratio of 1/18; see Fig. S12(a) in Sec. IX in the SM [29]). The supercell structure is relaxed using LSDA, and we compare the total energies calculated using LSDA + SOC + U for a spin orientation that is either out of plane or in plane and find that the magnetic anisotropy energy (MAE) still favors the easy out-of-plane orientation but drops drastically down to only 1.02 meV/Fe on average. This drastic reduction of MAE is mainly due to a lifting of the orbital degeneracy by the lattice distortion associated with the sulfur vacancy, and the additional crystal field splitting largely suppresses the orbital moment and the MAE. Note that the sulfur vacancy acts like an electron donor, and the minor gap in the otherwise vacancy-free prototype material closes now [see Fig. S12(b) in the SM]. Moreover, owing to the sulfur vacancy and the lattice distortion, there exist many inequivalent Fe sites in the supercell, and there are even much more different magnetic exchange parameters. Here we just make a crude estimate because of this complexity. For example, for the Fe site farthest away from the S vacancy, our LSDA + SOC + U calculations give the average first-nearest-neighbor exchange parameter of 6.00 meV. This small increase in the FM coupling strength, compared with the above homogeneous $J_1 = 5.81$ meV, may well be due to the enhanced itineracy associated with the electron donation of the sulfur vacancy. However, for the Fe site closest to the S vacancy, our LSDA + SOC + U calculations give an average first-nearest-neighbor exchange parameter of -5.70 meV, which even turns into the AFM type due to the S vacancy. Therefore, the average exchange (most likely FM) among the many different magnetic channels in the supercell with the sulfur vacancy can be expected to be no stronger than the homogeneous ones in the ideal lattice. Taking the above J_1 , J_2 , and J_3 as the upper limit, the drastic decrease in the MAE already significantly reduces T_C down to 90 K (see the solid black curve in Fig. 5). Such T_C would be further reduced (and would approach the experimental value of 15 K) when the averagely decreasing FM exchange (and even the AFM type for some exchange channels) is used. Therefore, to achieve the ideal high T_C in the FeS₂ monolayer, the S vacancy issue should be avoided during the sample preparation/growth, e.g., using high pressure [48], postgrowth treatment [49], and sulfur-rich growth [50].

IV. SUMMARY

In summary, we proposed that the FeS₂ monolayer is an appealing 2D high- T_C Ising ferromagnet using density functional calculations, crystal field level analyses and spin-orbital-state diagrams, RSWT, and MC simulations. Our results reveal that the unusual high-valence Fe⁴⁺ is in the LS L_{z+} spin-orbital ground state, resulting in a large orbital moment of about $1\mu_B$ and huge MA of 25 meV/Fe. The negative charge-transfer character associated with the Fe high valence, strong Fe 3d-S 3p hybridization, and wide bands but small band gap all help to establish a strong FM superexchange. As the compressive strains can further stabilize the L_{z+} ground state and enhance the FM couplings, our RSWT simulations showed that T_C of the FeS₂ monolayer increases

from 261 K for a bare monolayer up to 310–409 K under -2.5 to -5% strains. This work highlights the exploration of the spin-orbital degrees of freedom to produce strong Ising magnetism and FM coupling. This approach may pave the way for discovering more 2D high- T_C FM materials suitable for spintronic applications.

ACKNOWLEDGMENT

This work was supported by the National Natural Science Foundation of China (Grants No. 12104307, No. 12174062, and No. 12241402).

-
- [1] B. Huang, G. Clark, E. Navarro-Moratalla, D. R. Klein, R. Cheng, K. L. Seyler, D. Zhong, E. Schmidgall, M. A. McGuire, D. H. Cobden, W. Yao, D. Xiao, P. Jarillo-Herrero, and X. Xu, Layer-dependent ferromagnetism in a van der Waals crystal down to the monolayer limit, *Nature (London)* **546**, 270 (2017).
- [2] C. Gong, L. Li, Z. Li, H. Ji, A. Stern, Y. Xia, T. Cao, W. Bao, C. Wang, Y. Wang, Z. Q. Qiu, R. J. Cava, S. G. Louie, J. Xia, and X. Zhang, Discovery of intrinsic ferromagnetism in two-dimensional van der Waals crystals, *Nature (London)* **546**, 265 (2017).
- [3] T. Li, S. Jiang, N. Sivasdas, Z. Wang, Y. Xu, D. Weber, J. E. Goldberger, K. Watanabe, T. Taniguchi, C. J. Fennie, K. F. Mak, and J. Shen, Pressure-controlled interlayer magnetism in atomically thin CrI_3 , *Nat. Mater.* **18**, 1303 (2019).
- [4] T. Song, Z. Fei, M. Yankowitz, Z. Lin, Q. Jiang, K. Hwangbo, Q. Zhang, B. Sun, T. Taniguchi, K. Watanabe, M. A. McGuire, D. Graf, T. Cao, J.-H. Chu, D. H. Cobden, C. R. Dean, D. Xiao, and X. Xu, Switching 2D magnetic states via pressure tuning of layer stacking, *Nat. Mater.* **18**, 1298 (2019).
- [5] J. Li *et al.*, General synthesis of two-dimensional van der Waals heterostructure arrays, *Nature (London)* **579**, 368 (2020).
- [6] K. S. Burch, D. Mandrus, and J.-G. Park, Magnetism in two-dimensional van der Waals materials, *Nature (London)* **563**, 47 (2018).
- [7] T. Song, X. Cai, M. W.-Y. Tu, X. Zhang, B. Huang, N. P. Wilson, K. L. Seyler, L. Zhu, T. Taniguchi, K. Watanabe, M. A. McGuire, D. H. Cobden, D. Xiao, W. Yao, and X. Xu, Giant tunneling magnetoresistance in spin-filter van der Waals heterostructures, *Science* **360**, 1214 (2018).
- [8] N. D. Mermin and H. Wagner, Absence of ferromagnetism or antiferromagnetism in one- or two-dimensional isotropic Heisenberg models, *Phys. Rev. Lett.* **17**, 1133 (1966).
- [9] J. L. Lado and J. Fernández-Rossier, On the origin of magnetic anisotropy in two dimensional CrI_3 , *2D Mater.* **4**, 035002 (2017).
- [10] C. Xu, J. Feng, H. Xiang, and L. Bellaiche, Interplay between Kitaev interaction and single ion anisotropy in ferromagnetic CrI_3 and CrGeTe_3 monolayers, *npj Comput. Mater.* **4**, 57 (2018).
- [11] D.-H. Kim, K. Kim, K.-T. Ko, J. H. Seo, J. S. Kim, T.-H. Jang, Y. Kim, J.-Y. Kim, S.-W. Cheong, and J.-H. Park, Giant magnetic anisotropy induced by ligand LS coupling in layered Cr compounds, *Phys. Rev. Lett.* **122**, 207201 (2019).
- [12] K. Yang, F. Fan, H. Wang, D. I. Khomskii, and H. Wu, VI_3 : A two-dimensional Ising ferromagnet, *Phys. Rev. B* **101**, 100402(R) (2020).
- [13] Z. Lin, B. Huang, K. Hwangbo, Q. Jiang, Q. Zhang, Z. Liu, Z. Fei, H. Lv, A. Millis, M. McGuire, D. Xiao, J.-H. Chu, and X. Xu, Magnetism and its structural coupling effects in 2D Ising ferromagnetic insulator VI_3 , *Nano Lett.* **21**, 9180 (2021).
- [14] Y. Hao, Y. Gu, Y. Gu, E. Feng, H. Cao, S. Chi, H. Wu, and J. Zhao, Magnetic order and its interplay with structure phase transition in van der Waals ferromagnet VI_3 , *Chin. Phys. Lett.* **38**, 096101 (2021).
- [15] A. De Vita, T. T. P. Nguyen, R. Sant, G. M. Pierantozzi, D. Amoroso, C. Bigi, V. Polewczyk, G. Vinai, L. T. Nguyen, T. Kong, J. Fujii, I. Vobornik, N. B. Brookes, G. Rossi, R. J. Cava, F. Mazzola, K. Yamauchi, S. Picozzi, and G. Panaccione, Influence of orbital character on the ground state electronic properties in the van der Waals transition metal iodides VI_3 and CrI_3 , *Nano Lett.* **22**, 7034 (2022).
- [16] K. Yang, G. Wang, L. Liu, D. Lu, and H. Wu, Triaxial magnetic anisotropy in the two-dimensional ferromagnetic semiconductor CrSBr , *Phys. Rev. B* **104**, 144416 (2021).
- [17] D. Lu, L. Liu, Y. Ma, K. Yang, and H. Wu, A unique electronic state in a ferromagnetic semiconductor FeCl_2 monolayer, *J. Mater. Chem. C* **10**, 8009 (2022).
- [18] C. Huang, J. Feng, F. Wu, D. Ahmed, B. Huang, H. Xiang, K. Deng, and E. Kan, Toward intrinsic room-temperature ferromagnetism in two-dimensional semiconductors, *J. Am. Chem. Soc.* **140**, 11519 (2018).
- [19] F. Xue, Y. Hou, Z. Wang, and R. Wu, Two-dimensional ferromagnetic van der Waals CrCl_3 monolayer with enhanced anisotropy and Curie temperature, *Phys. Rev. B* **100**, 224429 (2019).
- [20] L. Liu, K. Yang, G. Wang, and H. Wu, Two-dimensional ferromagnetic semiconductor VBr_3 with tunable anisotropy, *J. Mater. Chem. C* **8**, 14782 (2020).
- [21] J. Zhou *et al.*, Composition and phase engineering of metal chalcogenides and phosphorous chalcogenides, *Nat. Mater.* **22**, 450 (2023).
- [22] M. M. Otrokov *et al.*, Prediction and observation of an anti-ferromagnetic topological insulator, *Nature (London)* **576**, 416 (2019).
- [23] Y. Deng, Y. Yu, M. Z. Shi, Z. Guo, Z. Xu, J. Wang, X. H. Chen, and Y. Zhang, Quantum anomalous Hall effect in intrinsic magnetic topological insulator MnBi_2Te_4 , *Science* **367**, 895 (2020).
- [24] H. Seki, Y. Hosaka, T. Saito, M. Mizumaki, and Y. Shimakawa, Ferromagnetism induced by substitution of the iron(IV) ion by an unusual high-valence nickel(IV) ion in antiferromagnetic SrFeO_3 , *Angew. Chem., Int. Ed.* **55**, 1360 (2016).
- [25] Y. Hosaka, N. Ichikawa, T. Saito, P. Manuel, D. Khalyavin, J. P. Attfield, and Y. Shimakawa, Two-dimensional charge disproportionation of the unusual high valence state Fe^{4+} in a layered double perovskite, *J. Am. Chem. Soc.* **137**, 7468 (2015).
- [26] M. Goto, T. Oguchi, and Y. Shimakawa, Geometrical spin frustration and monoclinic-distortion-induced spin canting in the double perovskites $\text{Ln}_2\text{LiFeO}_6$ ($\text{Ln} = \text{La}, \text{Nd}, \text{Sm}, \text{and Eu}$) with unusually high valence Fe^{5+} , *J. Am. Chem. Soc.* **143**, 19207 (2021).

- [27] G. Kresse and J. Hafner, *Ab initio* molecular dynamics for liquid metals, *Phys. Rev. B* **47**, 558(R) (1993).
- [28] J. P. Allen and G. W. Watson, Occupation matrix control of d- and f-electron localisations using DFT + U, *Phys. Chem. Chem. Phys.* **16**, 21016 (2014).
- [29] See Supplemental Material at <http://link.aps.org/supplemental/10.1103/PhysRevB.109.014431> for more details on (I) the trigonal crystal field and orbital state, (II) the LSDA + SOC + U results, (III) hybrid functional results, (IV) the exchange parameters, (V) two major superexchange channels, (VI) the renormalized spin-wave theory, (VII) strain results, (VIII) the Monte Carlo simulations, and (IX) the sulfur vacancy calculations. It also contains Refs. [21,30–37].
- [30] P. Blaha, K. Schwarz, F. Tran, R. Laskowski, G. K. H. Madsen, and L. D. Marks, Wien2k: An APW + lo program for calculating the properties of solids, *J. Chem. Phys.* **152**, 074101 (2020).
- [31] A. D. Becke, A new mixing of Hartree-Fock and local density-functional theories, *J. Chem. Phys.* **98**, 1372 (1993).
- [32] A. D. Becke, Density-functional thermochemistry. IV. A new dynamical correlation functional and implications for exact-exchange mixing, *J. Chem. Phys.* **104**, 1040 (1996).
- [33] J. P. Perdew, M. Ernzerhof, and K. Burke, Rationale for mixing exact exchange with density functional approximations, *J. Chem. Phys.* **105**, 9982 (1996).
- [34] F. Tran, P. Blaha, K. Schwarz, and P. Novák, Hybrid exchange-correlation energy functionals for strongly correlated electrons: Applications to transition-metal monoxides, *Phys. Rev. B* **74**, 155108 (2006).
- [35] P. Novák, J. Kuneš, L. Chaput, and W. E. Pickett, Exact exchange for correlated electrons, *Phys. Status Solidi B* **243**, 563 (2006).
- [36] Z. Li, T. Cao, and S. G. Louie, Two-dimensional ferromagnetism in few-layer van der Waals crystals: Renormalized spin-wave theory and calculations, *J. Magn. Magn. Mater.* **463**, 28 (2018).
- [37] N. Metropolis and S. Ulam, The Monte Carlo method, *J. Am. Stat. Assoc.* **44**, 335 (1949).
- [38] Q. Yao, J. Li, and Q. Liu, Fragile symmetry-protected half metallicity in two-dimensional van der Waals magnets: A case study of monolayer FeCl₂, *Phys. Rev. B* **104**, 035108 (2021).
- [39] X. Ou, H. Wang, F. Fan, Z. Li, and H. Wu, Giant magnetic anisotropy of Co, Ru, and Os adatoms on MgO (001) surface, *Phys. Rev. Lett.* **115**, 257201 (2015).
- [40] T. Mizokawa, H. Namatame, A. Fujimori, K. Akeyama, H. Kondoh, H. Kuroda, and N. Kosugi, Origin of the band gap in the negative charge-transfer-energy compound NaCuO₂, *Phys. Rev. Lett.* **67**, 1638 (1991).
- [41] V. Bisogni, S. Catalano, R. J. Green, M. Gibert, R. Scherwitzl, Y. Huang, V. N. Strocov, P. Zubko, S. Balandeh, J.-M. Triscone, G. Sawatzky, and T. Schmitt, Ground-state oxygen holes and the metal-insulator transition in the negative charge-transfer rare-earth nickelates, *Nat. Commun.* **7**, 13017 (2016).
- [42] R. B. Wexler, G. S. Gautam, E. B. Stechel, and E. A. Carter, Factors governing oxygen vacancy formation in oxide perovskites, *J. Am. Chem. Soc.* **143**, 13212 (2021).
- [43] C. Lu and J.-M. Liu, The $J_{\text{eff}} = 1/2$ antiferromagnet Sr₂IrO₄: A golden avenue toward new physics and functions, *Adv. Mater.* **32**, 1904508 (2020).
- [44] L. Wang, X. Zhang, H. L. Chan, F. Yan, and F. Ding, Formation and healing of vacancies in graphene chemical vapor deposition (CVD) growth, *J. Am. Chem. Soc.* **135**, 4476 (2013).
- [45] H. Wang, D. Yong, S. Chen, S. Jiang, X. Zhang, W. Shao, Q. Zhang, W. Yan, B. Pan, and Y. Xie, Oxygen-vacancy-mediated exciton dissociation in BiOBr for boosting charge-carrier-involved molecular oxygen activation, *J. Am. Chem. Soc.* **140**, 1760 (2018).
- [46] T. Kong, K. Stolze, E. I. Timmons, J. Tao, D. Ni, S. Guo, Z. Yang, R. Prozorov, and R. J. Cava, VI₃—A new layered ferromagnetic semiconductor, *Adv. Mater.* **31**, 1808074 (2019).
- [47] D. Ni, X. Gui, K. M. Powderly, and R. J. Cava, Honeycomb-structure RuI₃, a new quantum material related to α -RuCl₃, *Adv. Mater.* **34**, 2106831 (2022).
- [48] L. Yan, J. Qin, B. Liang, S. Gao, B. Wang, J. Cui, A. Bolag, and Y. Yang, High pressure rapid synthesis of LiCrTiO₄ with oxygen vacancy for high rate lithium-ion battery anodes, *Small* **18**, 2202901 (2022).
- [49] X. Zhao, P. Song, C. Wang, A. C. Riis-Jensen, W. Fu, Y. Deng, D. Wan, L. Kang, S. Ning, J. Dan, T. Venkatesan, Z. Liu, W. Zhou, K. S. Thygesen, X. Luo, S. J. Pennycook, and K. P. Loh, Engineering covalently bonded 2D layered materials by self-intercalation, *Nature (London)* **581**, 171 (2020).
- [50] X. Zheng, A. Calò, T. Cao, X. Liu, Z. Huang, P. M. Das, M. Drndic, E. Albisetti, F. Lavini, T.-D. Li, V. Narang, W. P. King, J. W. Harrold, M. Vittadello, C. Aruta, D. Shahrjerdi, and E. Riedo, Spatial defects nanoengineering for bipolar conductivity in MoS₂, *Nat. Commun.* **11**, 3463 (2020).